Journal of Materials Chemistry C

Eco-friendly, solution-processable and efficient low-energy lighting phosphors: copper halide based hybrid semiconductors Cu4X6(L)2 (X = Br, I) composed of covalent, ionic and coordinate bonds

Journal:	*Journal of Materials Chemistry C*
Manuscript ID	TC-ART-09-2020-004672.R1
Article Type:	Paper
Date Submitted by the Author:	27-Oct-2020
Complete List of Authors:	Hei, Xiuze; Rutgers The State University of New Jersey, Chemistry and Chemical Biology Teat, Simon; Lawrence Berkeley National Laboratory, ALS Liu, Wei; Rutgers University, Chemistry and Chemical Biology Li, Jing; Rutgers The State University of New Jersey, Chemistry and Chemical Biology

ARTICLE

Eco-friendly, solution-processable and efficient low-energy lighting phosphors: copper halide based hybrid semiconductors $Cu_4X_6(L)_2$ (X = Br, I) composed of covalent, ionic and coordinate bonds

Received 00th January 20xx,
Accepted 00th January 20xx

DOI: 10.1039/x0xx00000x

Xiuze Hei,[a] Simon J. Teat,[b] Wei Liu,[a] Jing Li*,[a]

A series of copper halide based inorganic-organic hybrid simiconductors has been synthesiszed. Structural analysis confirms that all compounds are composed of one-dimensional $Cu_4X_6^{2-}$ anionic chains that coordinate to cationic ligands via Cu-N dative bonds. Different coordination affinity of the ligands leads to two types of ligand arrangement with various structural distortion. All compounds are highly resistent to heat and moisture as a result of as a result of combination of coordinate and ionic bonds. Low energy emission with high efficiency is achieved for these compounds and the emission energy (~552-615 nm) and color (yellow-orange) can be tuned by varing ligand and halogen element. The electronic strucutre and luminescence mechanism are examed by both experimental and theoretical methods. More importantly, all compounds demonstrate good solubility in polar aprotic solvents, a desired property that is absent in all other CuX hybrid families of extended structures, which is attributed primarily to the ionic nature of this material class. The good solution-processibility, cost effective and easily scalable synthesis coupled with high quantum efficiencies and framework stability make these hybrid materails promising phosphors for general lighting applications.

Introduction

Current white-Light-emitting-diodes (WLEDs) used for general lighting application are generally phosphor-converted WLEDs (pc-WLEDs), which are assembled by coating blue-excitable yellow (or multicomponent) phosphors onto blue LED chips to realize overall white emission.[1, 2] Yet while YAG:Ce^{3+} (the benchmark yellow phosphor) exhibits intensive yellow emission under blue light excitation, the WLEDs using this phosphor alone suffers from high correlated color temperature (CCT) thus is too "cold" for indoor lighting uses, as the emission spectrum of YAG:Ce^{3+} lacks low energy part.[1, 3, 4] In addition, nearly all commercial phosphors currently used in pc-WLEDs rely on rare-earth elements (REEs) which are subject to potential supply and cost risks, as well as severe environmental consequences caused by their mining and extraction processes.[5-9] Therefore, achieving low-energy emitting phosphors that are free of REEs and strongly blue-excitable with high quantum efficiency has been an on-going research topic of substantial interest.

Recently, copper(I) halide based inorganic-organic hybrid semiconductors as an important class of crystalline materials have risen to prominence due to their potential for use in REE-free solid-state lighting (SSL) devices.[10-21] The main advantages of this family of compounds, compared to commercial and other phosphor classes, lie in their cost-efficient and easily scalable synthesis, nontoxic nature, structural diversity, optical tunability, and strong photoluminescence.[13, 22] Generally, these compounds can be formulated as $Cu_xX_yL_z$ (where X = Cl, Br or I; L = N, S or P based organic ligands). In terms of chemical bonding between the inorganic components and ligands, they can be further divided into three subgroups.[11] The first subgroup contains the most explored neutral compounds, in which both the inorganic motif (Cu_xX_x) and organic ligand (L) are charge neutral and connected via Cu-L coordinate/dative bonds;[18-21, 23] the second subgroup is the pure ionic compounds, formed by co-crystallization of anionic inorganic and cationic organic motifs but without coordinate bonds between these building blocks.[24-28] Ionic ligands have also been used in forming anionic MOFs and show interesting structural directing effects.[29] Recently, we have developed a brand new subgroup using ligands deliberately designed to have both cationic centers (quaternary N or P atoms) and coordination-active sites toward Cu(I) atoms. The members of this subgroup are denoted as All-In-One (AIO) structures as they are composed of all three types of bonds, with covalent bonding within the inorganic motif, and both ionic and coordinate bonding between inorganic and organic motifs.[16, 17, 30, 31] The AIO-type compounds combine advantageous features of both neutral and ionic subgroups,

[a] Department of Chemistry and Chemical Biology, Rutgers University, Piscataway, New Jersey 08854, USA.
[b] Advanced Light Source, Lawrence Berkeley National Laboratory, Berkeley, CA 94720, USA

† Footnotes relating to the title and/or authors should appear here.
Electronic Supplementary Information (ESI) available: 1H NMR spectroscopic data, structural plots, crystal images, DFT calculation details and results. CCDC 1943651, 2032011 and 2032012. See DOI: 10.1039/x0xx00000x

including systematic bandgap tunability, enhanced thermal and chemical stability, high luminescence and greatly increased solubility and solution-processability.[16, 17, 30, 31] Therefore, AIO-type compounds are considered as the most promising candidates for REE-free phosphors.

Various CuI AIO compounds have been reported with their dimensionality ranges from 0D to 2D. Their emission energy can be tuned by either adjusting the lowest unoccupied molecular orbital (LUMO) of the ligands or varying the structure of $[Cu_xI_y]^{x-y}$ motifs. However, halogen substitution, as a feasible strategy used in tuning bandgap and emission energy of lead halide

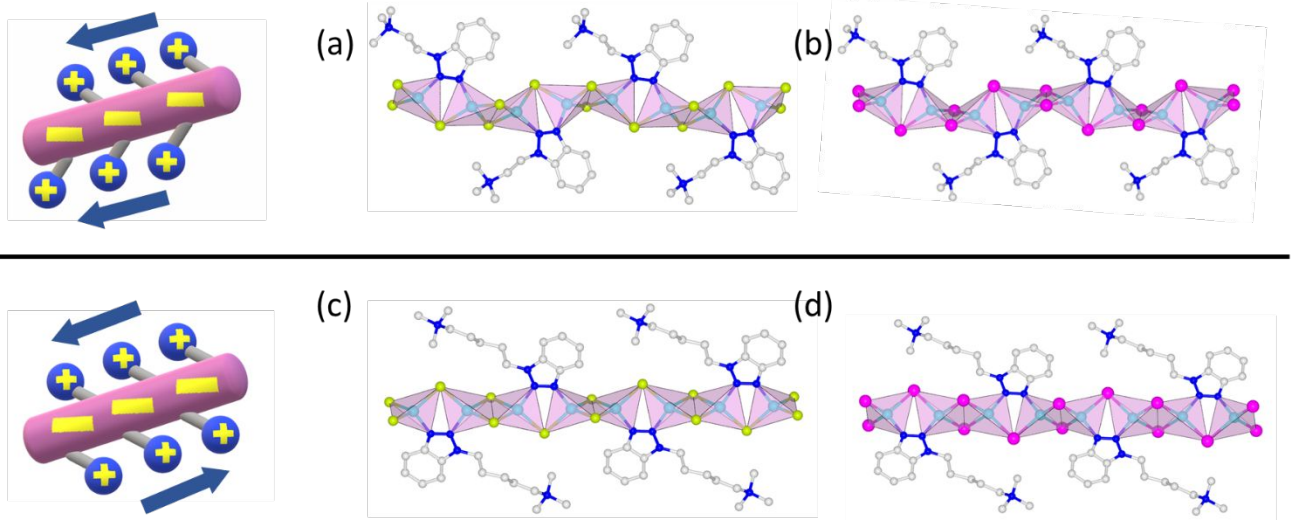

Figure 1. Crystal structures of title compounds, (a) **1**, (b) **2**, (c) **3** and (d) **4**. Images on the left (top: cis; bottom: trans) show relative orientations of the ligands on opposite site of the 1D-Cu_4X_6 chain. Color scheme: gray: C; blue: N; Cyan: Cu; lime: Br; purple: I. All H atoms are omitted for clarity.

perovskites[32-35] and pure inorganic copper halide[36-38] structures, has not been applied to the AIO system. CuBr based AIO-type compounds remain unexplored, as well as the halogen dependent optical properties of AIO-type compounds. Herein, we report four different 1D-AIO structures composed of 1D-$Cu_4X_6^{2-}$ (X = Br, I) inorganic chains and two benzotriazole based cationic ligands. Two types of ligand arrangements are found in these structures due to different binding affinity of ligands. The electronic structures and luminescence mechanism, as well as effect of halogen substitution on the photophysical properties of the AIO-type compounds are examined by both experimental and theoretical methods. All compounds remain stable up to 210 °C and are well soluble in polar aprotic solvents such as DMSO. They emit low-energy yellow-orange color (552-615 nm) with internal quantum yield (IQY) up to 70% and 64% excited by UV (360 nm) and blue (450 nm) light source, respectively.

Results and Discussion

Structure Description. The molecular structures of benzotriazole-based cationic ligands are shown in Fig. S1-S3 along with ^{1}H NMR data to confirm the purity. Reactions of these ligands with either CuBr or CuI afforded four one-dimensional (1D) chain AIO-type compounds, namely, three new structures **1-3** and one previously reported structure **4**.[16] The single crystal X-ray analysis reveals that these compounds share a common formula of $Cu_4X_6(L)_2$ (X = Br, I). Their crystal structures feature 1D inorganic anionic chains 1D-$Cu_4X_6^{2-}$ which are charge balanced by cationic ligands that also coordinate to the chains via Cu-N dative bonds (Fig. 1). Crystal data are summarized in Table 1. Within the inorganic chains, all copper atoms are tetrahedrally coordinated to three halogen atoms and one nitrogen atom from ligands, and all halogen atoms are bridging to two copper atoms. All CuX_3N tetrahedra are edge- and corner-sharing. Since each ligand has two N atoms available for Cu-N coordination, the title compounds adopt the μ^2-DC (dicoordination mode), in which 2 N atoms, 2 Cu atoms and a bridging halogen atom form a five-member ring. This interesting coordination mode has proven to form more rigid bonds and reduce luminescence decay by suppressing molecular motions such as vibrations and rotations.[16] The Cu-N bond lengths in these compounds range from 2.0-2.2 Å, comparable to those of similar structures.

While the inorganic chains are very similar in compounds **1**-**4**, the ligands on the opposite side of the chain adopt two different orientations. In compounds **1** and **2**, they orient in “cis” fashion (alkyl chains of the ligands on the opposite sides point to the same direction, Fig. 1, top left). In compounds **3**-**4**, however, they take the “trans” orientation, with these alkyl chains point to the opposite directions (Fig. 1, bottom left).

Such structural differences may arise from the different coordination ability of ligands. Due to the inductive effect,[39] electron density of the coordination-active N atoms can be reduced by strong electron withdrawing NR_4^+ center and N1 is affected more than N2 (Fig. 2a-b, Table S2). Therefore, longer

ARTICLE

Table 1. Summary of crystal data of compounds **1-4**.

Compound	1D-Cu_4Br_6(*bttme*)$_2$ (1)	1D-Cu_4I_6(*bttme*)$_2$ (2)	1D-Cu_4Br_6(*bttmpe*)$_2$ (3)	1D-Cu_4I_6(*bttmpe*)$_2$[16] (4)
Empirical Formula	$C_{22}H_{34}Cu_4Br_6N_8$	$C_{22}H_{34}Cu_4I_6N_8$	$C_{28}H_{46}Cu_4Br_6N_8$	$C_{28}H_{46}Cu_4I_6N_8$
FW	1144.19	1426.13	1228.35	1510.29
Space Group	P 2_1/n	P 2_1/n	P -1	P -1
a **(Å)**	16.5784(6)	17.0727(9)	8.9746(3)	9.3391(5)
b **(Å)**	12.8909(4)	13.2826(7)	10.9880(4)	11.1574(6)
c **(Å)**	17.2528(6)	18.0067(9)	11.0013(4)	11.4854(6)
α (°)	90	90	94.159(2)	93.313(3)
β (°)	116.812(1)	117.938(3)	109.727(1)	110.774(3)
γ (°)	90	90	106.277(1)	107.758(3)
V (Å^3)	3290.7(2)	3607.5(3)	963.35(6)	1046.98(10)
Z	4	4	1	1
T **(K)**	100	100	100	100(2)
λ(Å)	0.72880	0.72930	0.72880	0.7749
R_1	0.0177	0.0384	0.0203	0.0249
wR_2	0.0395	0.1355	0.0540	0.0498

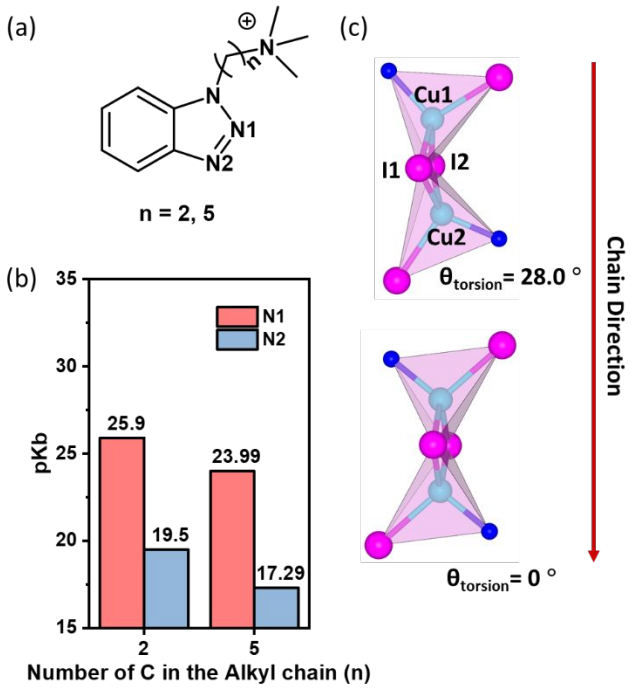

Figure 2. (a) Ligand structures used to calculate pK_b values of N1 and N2. (b) pK_b values of N1 and N2 in selected ligands. (c) The $Cu_2X_4N_2$ segment in **2** (top) and **4** (bottom), and the corresponding torsion/dihedral angles.

Cu-N1 and shorter Cu-N2 bonds are observed in all four compounds. This length difference in the two Cu-N bonds results in a distortion of the 1D-$Cu_4X_6^{2-}$ chain in a zig-zag manner. Such distortion is lessened when the length difference between Cu-N1 and Cu-N2 decreases as the result of increasing alkyl chain length of the ligand from n = 2 to 5 (Table 2). Using Compound **2** (n = 2) as an example, the Cu-N1 bond (2.104 Å) is ~0.08 Å longer than the Cu-N2 bond (2.027 Å), forcing the inorganic backbone into a more zig-zag form with a dihedral/torsion angle ($\theta_{torsion}$) of 28.0° (Fig. 2c, top), and a cis orientation of the ligands. The difference between the two Cu-N bonds becomes negligible with compound **4** (~0.01 Å), due to significantly weakened inductive effect with longer alkyl chain (n = 5), which results in a "zero" dihedral/torsion angle (Fig. 2c, bottom) and a "flattened" chain, allowing a trans orientation of the ligands. (Table 2 and Fig. 1b, 1d).

Table 2. Selected bond lengths and angles of compounds **1**-**4**.

	1	2	3	4
$L_{N1\text{-}Cu}$ (Å)	2.068	2.104	2.068	2.069
$L_{N2\text{-}Cu}$ (Å)	2.028	2.027	2.036	2.058
$\Delta L_{N\text{-}Cu}$ (Å)	0.040	0.077	0.032	0.011
θ_{tor} (°)	27.5	28.0	0	0

$\Delta L_{N\text{-}Cu} = L_{N1\text{-}Cu} - L_{N2\text{-}Cu}$

$\theta_{torsion}$= torsion angle or dihedral angle Cu1-I1-I2-Cu2

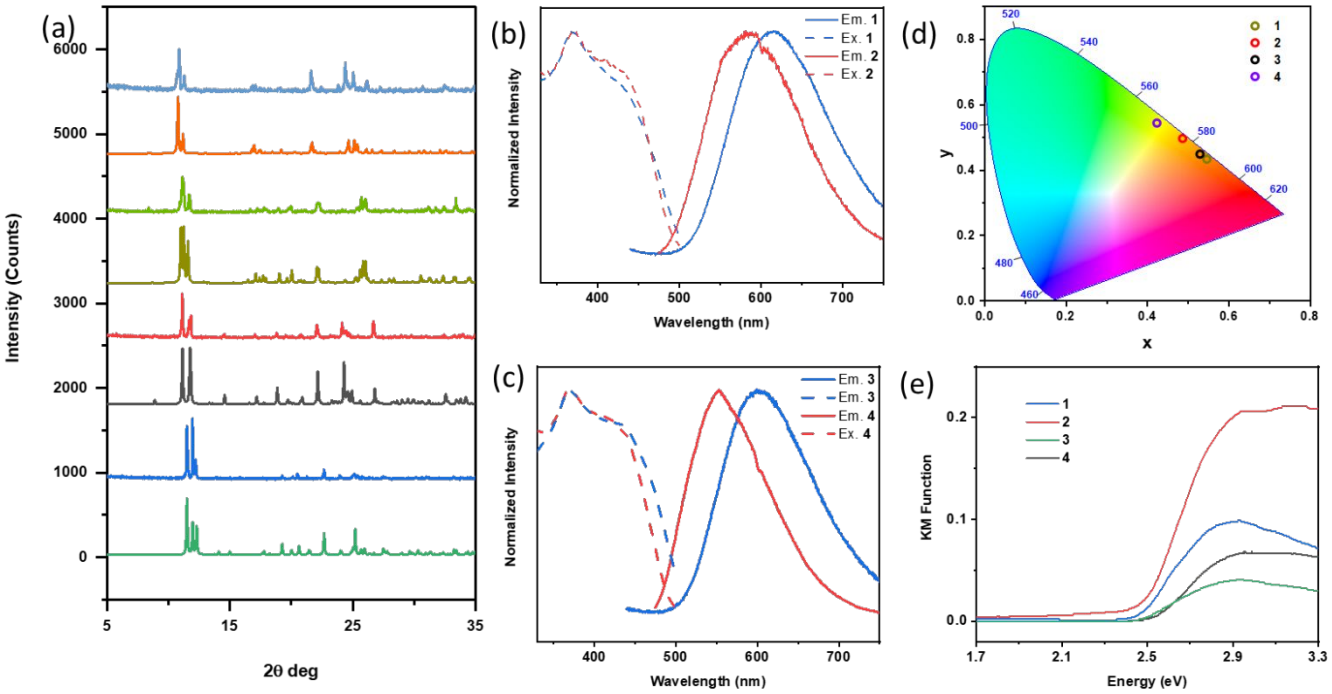

Figure 3. (a) PXRD patterns of compounds **1**-**4**. From bottom to top: simulated **1**, as made **1**; simulated **2**, as made **2**; simulated **3**, as made **3**; simulated **4**, as made **4**. Normalized excitation and emission spectra of (b) **1** and **2**, (c) **3** and **4**. All data were recorded at room temperature. All emission spectra were measured at λ_{ex} = 360 nm and all excitation spectra were collected using their emission maximum. (d) Color chromaticity (λ_{ex} = 360 nm) and (e) optical absorption spectra of compounds **1–4**.

Table 3. Summary of important physical properties of compounds **1**-**4**.

#	Formula	Band Gap (eV)	Emission (nm)	CIE	IQY (%) λ_{ex} = 360 nm	IQY (%) λ_{ex} = 450 nm	T_d(°C)	Solubility (mg/ml@RT)
1	$Cu_4Br_6(bttme)_2$	2.5	615	(0.55, 0.43)	56	44	220	110
2	$Cu_4I_6(bttme)_2$	2.45	585	(0.49, 0.49)	69	57	210	200
3	$Cu_4Br_6(bttmpe)_2$	2.5	600	(0.53, 0.46)	69	60	250	40
4	$Cu_4I_6(bttmpe)_2$	2.5	552	(0.43, 0.54)	70	64	235	80

Photophysical Properties. The phase purity of all four compounds was confirmed by PXRD analysis as shown in Fig. 3a. Their photophysical properties were investigated using photoluminescence emission spectroscopy as well as UV-vis optical absorption spectroscopy at room temperature. The important photophysical properties are summarized in Table 3. All title compounds emit low energy lights between 552 and 615 nm, and can well be excited by blue light. The emission color ranges from yellow with Commission International del'Eclairage (CIE) Color Coordinates (x, y) of (0.43, 0.54) to orange with CIE of (0.55, 0.43) (Fig. 3b-d). The internal quantum yields (IQYs) of **1**-**4** were determined at room temperature using 360 nm and 450 nm as excitation wavelength. The highest values are 70% (λex = 360 nm) and 64% (λex = 450 nm), suggesting their potential for use as low energy phosphors in blue chip based pc-WLEDs. Confirmed by the room temperature solid state photoluminescence (PL) experiments, emission profile of all four compounds demonstrates single band feature with a full width at half maximum (FWHM) around 150 nm, characteristic of a dominating (M+X)LCT process.[10, 18, 40, 41] Optical absorption spectra for compounds **1-4** were recorded at room temperature and converted to the Kubelka-Munk function (Fig. 3e). The optical bandgaps were estimated from their absorption edges. Generally, the bandgaps of bromide based compounds are slightly larger than their corresponding iodide based compounds. However, all bromide-based structures exhibit red-shifted emission compared to their iodide-based analogues. For example, compound **1** has a slightly higher bandgap than that of compound **2** but its emission is redshifted by 30 nm with

respect to the latter. This behavior has been observed in a number of other copper halide based hybrid structures.[42-44]

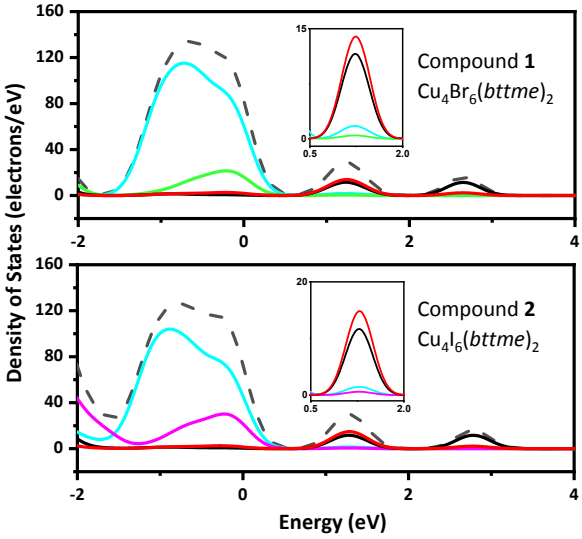

Figure 4. Total density of states (DOS) and projected density of states (PDOS) for compounds **1** and **2**. Line color scheme: dashed black: total; cyan: Cu (3d); green: Br (4p); purple: I (5p); black: C (2p); red: N (2p). Inset: conduction band minimum region.

Electronic Band Structures and Emission Mechanisms. To understand the as well as the electronic structures of these compounds and to gain insight of the origin of emission, band structures (BS) and density of states (DOS) calculations were carried out using the CASTEP package.[45] The results are summarized in Table S2. The calculated projected DOS (PDOS) shows that all compounds share the same features: the contribution to the valence band maximum (VBM) are primarily from the inorganic components, namely Cu 3d, I 5p or Br 4p; While for the conduction band minimum (CBM), the contributions largely come from the organic motifs, specifically C 2p and N 2p orbitals (Fig. 4, Fig. S8). These results suggest a combination of metal-to-ligand charge transfer (MLCT) and halide-to-ligand charge transfer (XLCT), or (M+X)LCT mechanism for all the compounds. This is similar to other copper iodide based AIO compounds.[16, 17, 30]

Further analysis of the calculated VBM region reveals that i) Cu orbitals contribute much more than halogen atomic orbitals, indicating MLCT may dominate the excitation process; ii) Br-based compounds demonstrate less halogen contribution to the VBM, compared to their I-based counterparts. For example, compound **1** shows a distribution of 84.4% and 12.4% of Cu and Br atomic orbitals in its VBM, while the VBM of compound **2** has a partition of 77.4% and 19.4% of Cu and I atomic orbitals, respectively. Similar features have been observed in the charge-neutral Cu_2X_2 dimer cluster based hybrid materials.[46] Br^- has a relatively stronger ligand field strength compared to I^-, and thus, can increase the splitting of the Cu 3d orbitals, leading to a smaller MLCT excited state energy and red-shifted emission.[42, 47, 48] However, such red-shifting effect suffers from a sacrifice of IQYs. I-based compounds exhibit greater XLCT contributions to their lowest excited states than those of their Br-based counterparts. Due to the more significant participation of I 5p orbital in the excited state transitions and larger atomic number of I atoms, stronger spin-orbit coupling may be present in the copper iodide hybrid compounds, leading to enhanced intersystem crossing (ISC) relative to that of the Br-based compounds. Due to the much faster transition time of $S_1 \rightarrow T_1$ (order of 10 ps) in Cu(I) compounds, the T_1 and S_1 excitation states of compounds reach thermal equilibration rapidly upon excitation.[49] Therefore, with enhanced transition of $T_1 \rightarrow S_0$, shortened overall decay time can be expected and lead to improved quantum yield.[44, 50] Previous studies have shown that I-based compounds usually afford narrower energy gap between S_1 and T_1 ($\Delta E(S_1 - T_1)$) than lighter halogens, resulting in manifested TADF and thus higher IQYs.[47, 51]

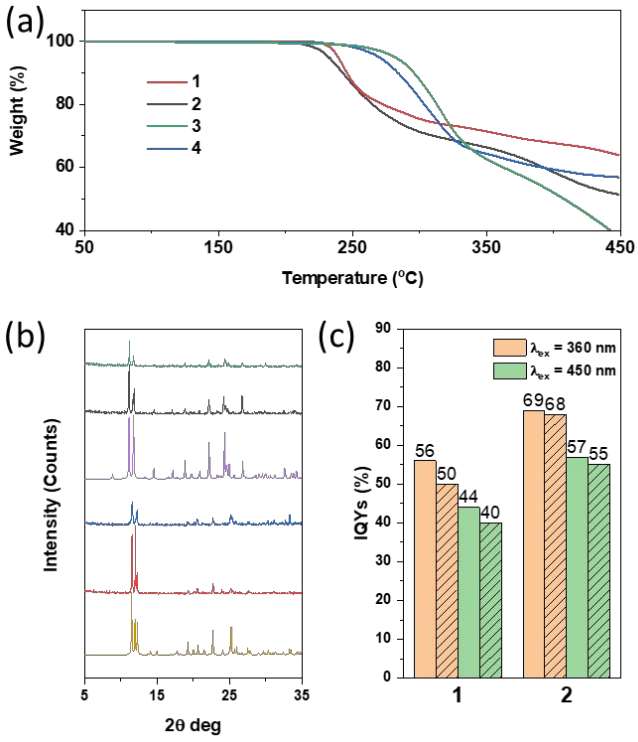

Figure 5. (a) TG plots of compounds **1-4**. (b) PXRD patterns of samples at different conditions. From bottom to top: Simulated **1**, as made **1**, compound **1** after 3 months under ambient atmosphere, simulated **2**, as made **2**, compound **2** after 3 months under ambient atmosphere. (c) IQYs measured before (unshaded areas) and after (shaded areas) exposed to air for 3 months.

Stability and Solubility. The enhancement of thermal stability of the AIO compounds, namely having both ionic bonds and dative bonds between the inorganic and organic components, is reflected from the results of thermogravimetric analysis (TGA). Compared to charge-neutral 1D-CuI(*L*) staircase chain based structures which generally decompose below 150 °C,[10] all

title compounds are stable up to at least 210 °C with some reaching 250 °C (Fig. 5a), similar to those previously reported 1D-AIO compounds.[16] In general, Br-based compounds show about 10 °C thermal stability enhancement to their I-based counterparts. This can be ascribed to stronger electronegativity of Br, which gives rise to stronger Cu-Br bond than Cu-X bond. In addition, it further reduces the electron density of Cu atoms and enhances Cu-N dative bonds[44, 52], which also agrees with the relatively short Cu-N bonds in Br-based structures (Table 2).

Air/moisture stability of these compounds was evaluated using compounds **1** and **2**, two least thermally stable members of the group, based on the TG results (Fig. 5a). After exposure under ambient conditions for three months, both samples remain highly crystalline without sign of decomposition or impurity phase formation (Fig. 5b). Small decrease in their IQYs was observed, and for compound **2**, such decrease is nearly negligible (Fig. 5c).

Another important feature of AIO compounds is their high solubility in polar aprotic solvents such as DMSO. Unlike other types of hybrid network structures based on charge-neutral Cu_mI_m, which are known to be insoluble in any organic and inorganic solvents and thus unsuitable for low-cost and large-scale solution-based fabrication processes,[10, 18] all title compounds show good solubility in DMSO (Table 3), similar to other AIO compounds reported to date.[16, 17, 30]

To investigate the solvation behaviour of the title compounds, we evaluated ^{1}H NMR of the DMSO solutions of compounds **2** and **4** (Figs. S3-4). Its NMR spectrum shows characteristic peaks of the ligand with some differences: i) the peaks of protons near cationic centre shifted to upfield compared to the free ligands. For the free ligands, the X^- anion is close to the cationic centre, extracting electron density from it thus shifting the peaks to slightly lower field. However, such effect is absent in the DMSO solution of dissolved hybrid compound, suggesting weakened interaction between the cationic centre of ligands and free X^-; ii) Larger chemical shift difference between the H3 and H6 signals compared to those in free ligands was observed. This may be attributed to the Cu atoms that are still bound to the N atoms which alters the chemical environment of H atoms. Therefore, the dissolved species can be pictured as small fragments composed of CuX clusters and ligands, and they remain coordinated via Cu-N dative bonds. This agrees with the electrospray ionization mass spectrometry (ESI-MS) study carried out in an earlier study.[30]

Experimental Section

Material. CuI (98%, Alfa Aesar); CuBr (98%, Alfa Aesar); 1H-benzo[d][1,2,3]triazole (99%, Alfa Aesar); 1-bromo-2-chloropropane (98%, Alfa Aesar); 1,2-Dibromoethane (98%, Alfa Aesar); 1-bromo-5-chloropentane (98%, Alfa Aesar); 1,5-Dibromopentane (98%, Alfa Aesar); trimethylamine (33% w/w in ethanol, Alfa Aesar); potassium carbonate (99%, Sigma-Aldrich); potassium iodide (99%, Alfa Aesar); acetone (99.5%, VWR); acetonitrile (99.5%, VWR); ethyl ether (99%, Fisher); Methanol (99%, Alfa Aesar); Dimethyl sulfoxide (99%, Alfa Aesar); sodium salicylate (99%, Merck) and YAG:Ce^{3+} type 9800 (Global Tungsten & Powders Corp).

Preparation of 1-(2-chloroethyl)-1H-benzo[d][1,2,3]triazole (*Cl-ebt*). Benzotriazole (*bta*) (3.0 g, 0.025 mol) was dissolved in acetonitrile (250 ml), K_2CO_3 (4.1 g, 0.030 mol) and 1-bromo-2-chloroethane (2.1 ml 0.025 mol) were added to the reaction at room temperature. The mixture was kept stirring for 2 days before the solution was filtered. The filtrate was evaporated under reduced pressure, and then purified by column chromatography, giving white crystalline powder as *Cl-ebt*. The yield is 65%.

Preparation of 1-(2-bromoethyl)-1H-benzo[d][1,2,3]triazole (*Br-ebt*). *Br-ebt* was synthesized with similar procedure as *Cl-ebt* but using 1,2-Dibromoethane. White crystalline powder was obtained as *Br-ebt*. The yield is 45%.

Preparation of 1-(5-bromopentyl)-1H-benzo[d][1,2,3]triazole (*Br-pebt*). Oil-like liquid was obtained as *Br-pebt* under similar condition as that of *Cl-pebt,* using 1,5-Dibromopentane as alkylation reagent. The yield is 52%.

Preparation of 2-(1H-benzo[d][1,2,3]triazol-1-yl)-N,N,N-trimethylethan-1-aminium Bromide (*bttme* Br). *Br-ebt* (2.2 g, 0.01 mol) was dissolved with 100 ml acetonitrile and then trimethylamine (33 wt% in ethanol solution 7.1 ml) was added. After stirring under 60 °C for 3 days, the solvent was removed under reduced pressure to give crude product. Washing with ethyl ether several times and recrystalized with ethanol affords white crystalline compounds as pure *bttme* Br. The yield is 60%.

Preparation of 2-(1H-benzo[d][1,2,3]triazol-1-yl)-N,N,N-trimethylethan-1-aminium iodide (*bttme* I). *Cl-ebt* (1.8 g, 0.01 mol) was fully dissolved in acetone (100 ml) and then KI (2 g) was added into the solution. The mixture was stirred for 2 h at room temperature before the solution was filtered. The filtrate was evaporated under reduced pressure then added with acetonitrile (100 ml) and trimethylamine (33 wt% in ethanol solution 7.1 ml). The precipitate was formed after stirring under 60 °C for 2 days. The reaction mixture was evaporated under reduced pressure, washed with ethyl ether and dried under vacuum as the final product. The yield is 55%.

Preparation of 5-(1H-benzo[d][1,2,3]triazol-1-yl)-N,N,N-trimethylpentan-1-aminium Bromide (*bttmpe* Br). *Br-pebt* (2.7 g, 0.01 mol) and trimethylamine (33 wt% in ethanol solution 7.1 ml) were added to acetonitrile (100 ml) and stirred at 60 °C for 3 days before removal of solvent under reduced pressure. The mixture was washed with ethyl ether and recrystallized with ethanol to give white crystalline powder as pure *bttmpe* Br. the yield is 61%.

Synthesis of 1D-Cu_4Br_6(*bttme*)$_2$ (1). CuBr (0.022 g, 0.15 mmol), and ligand *bttme* Br (0.029 g, 0.1 mmol) were sealed in a Pyrex tube with MeOH (2.5 ml) and DMSO (0.5 ml) as solvents. The reaction tube was heated in a 120 °C oven for two days. Yellow needle-shaped single crystals were formed and collected by filtration.

Synthesis of 1D-Cu_4I_6(*bttme*)$_2$ (2). CuI (0.038 g, 0.2 mmol) was first dissolved in KI saturated solution (2 ml) in a reaction vial. Acetonitrile (2 ml) was added as another layer and then the ligand *bttme* I (33 mg, 0.1 mmol) in methanol (2 ml) was added

slowly into the vial. The reaction mixture was kept undisturbed at room temperature, and block-like single crystals along with crystalline powder were collected by filtration after 3 days.

Synthesis of 1D-Cu_4Br_6(*bttmpe*)$_2$ (3). Compound **3** was synthesized similar to **1** except *bttmpe* Br was used as ligand. Yellow plate-like single crystals were collected after filtration.

Synthesis of 1D-Cu_4I_6(*bttmpe*)$_2$ (4). Compound **4** was synthesized according to the reported procedures.[16]

Single crystal X-ray diffraction (SCXRD). Single crystal data of **1**-**3** were collected on a D8 goniostat equipped with a Bruker PHOTON100 CMOS detector at the Advanced Light Source (ALS), Lawrence Berkeley National Laboratory, using synchrotron radiation. The structures were solved by direct methods and refined by full-matrix least-squares on F^2 using the Bruker SHELXTL package. These data can be obtained free of charge from The Cambridge Crystallographic Data Centre via www.ccdc.cam.ac.uk/data_request/cif. The structures were deposited in Cambridge Crystallographic Data Centre (CCDC) with numbers 1943651, 2032011-2032012.

Powder X-ray Diffraction (PXRD) Analysis. Powder X-ray diffraction (PXRD) analyses were carried out on a Rigaku Ultima-IV unit using Cu Kα radiation (λ = 1.5406 Å). The data were collected at room temperature in a 2ϑ range of 3–40° with a scan speed of 2°/ min. The operating power was 40 kV/40 mA.

Room-Temperature Photoluminescence Measurements. Photoluminescence (PL) measurements were carried out on a Horiba Duetta fluorescence spectrophotometer. Powder samples were evenly distributed and sandwiched between two glass slides (which do not have emission in the visible range) for room temperature measurements.

Thermogravimetric Analysis. Thermogravimetric analyses (TGA) of samples were performed using the TA Instrument Q5000IR thermalgravimetric analyser with nitrogen flow and sample purge rate at 10 and 12 mL/min, respectively. About 3 mg of samples were loaded onto a platinum sample pan and heated from room temperature to 450 °C at a rate of 10 °C/min under nitrogen flow.

Diffuse Reflectance Spectroscopy. Optical absorption spectra were measured at room temperature on a Shimadzu UV-3600 UV−vis−NIR spectrometer. The reflectance data were converted to Kubelka−Munk function, $\alpha/S = (1 - R)^2 /2R$ (α is absorption coefficient, R is reflectance and S is scattering coefficient. S was treated as a constant since the average particle size of samples is significantly larger than 5 μm).

Internal Quantum Yield (IQY) Measurements. IQY measurements were made on C9920−02 absolute quantum yield measurement system (Hamamatsu Photonics) with 150 W xenon monochromatic light source and 3.3 in. integrating sphere. Sodium salicylate (SS) and YAG:Ce^{3+} were chosen as the standards with reported IQY values of 60% and 95% at an excitation energy of 360 and 450 nm, respectively. Their IQY values were measured to be 64% and 96%, respectively, and corrections were made based on the reported data.

DFT Calculations. Electronic bandgaps and density of states (DOS) were calculated using Cambridge Serial Total Energy Package (CASTEP) in Materials studio. The pK_a and pK_b values of ligands were calculated using (B3LYP/6-31+G(d)) as implemented in Gaussian 16. The HOMO and LUMO energies of ligands were calculated using Gaussian 09 with B3LYP/6-31+G(d) basis set. All the calculation details can be found in Supporting Information.

Conclusions

In summary, a series of stable, solution processable and highly emissive hybrid materials made of 1D-$Cu_4X_6^{2-}$ (X = I, Br) anionic chains and benzotriazole based cationic ligands have been synthesized and structurally characterized. The inorganic components are made of earth-abundant and eco-friendly elements that do not involve highly pollutive and hazardous mining as in the cases of REEs,[7-9, 53] All AIO-type compounds exhibit excellent moisture and thermal stability with decomposition temperatures above 210 °C. They remain highly crystalline after 3 months exposure to air. All compounds emit bright yellow-orange color (552-615 nm) with high internal quantum yield (IQY) in the range of 70% and 60% when excited by UV (360 nm) and blue (450 nm) light source, respectively. Low-energy emission, high efficiency and robustness of these compounds, coupled with low cost and easily scalable synthesis and good solution processability make them promising candidates as eco-friendly alternative phosphors for general lighting devices.

Conflicts of interest

There are no conflicts to declare.

Acknowledgements

The Advanced Light Source (ALS) was supported by the Director, Office of Science, Office of Basic Energy Science, of the U.S. Department of Energy, under contract DE-AC02-05CH11231.

Notes and references

1. X. Huang, *Nat. Photon.*, 2014, **8**, 748-749.
2. Y. H. Kim, P. Arunkumar, S. H. Park, H. S. Yoon and W. B. Im, *Mater. Sci. Eng. B*, 2015, **193**, 4-12.
3. H. Zhu, C. C. Lin, W. Luo, S. Shu, Z. Liu, Y. Liu, J. Kong, E. Ma, Y. Cao, R.-S. Liu and X. Chen, *Nat. Commun.*, 2014, **5**, 4312.
4. W. Liu, D. Banerjee, F. Lin and J. Li, *J. Mater. Chem. C*, 2019, **7**, 1484-1490.
5. Q. Gong, Z. Hu, B. J. Deibert, T. J. Emge, S. J. Teat, D. Banerjee, B. Mussman, N. D. Rudd and J. Li, *J. Am. Chem. Soc.*, 2014, **136**, 16724-16727.
6. F. Lin, H. Wang, W. Liu and J. Li, *J. Mater. Chem. C*, 2020, **8**, 7300-7303.
7. A. R. Chakhmouradian and F. Wall, *Elements*, 2012, **8**, 333-340.
8. T. Dutta, K.-H. Kim, M. Uchimiya, E. E. Kwon, B.-H. Jeon, A. Deep and S.-T. Yun, *Environ. Res.*, 2016, **150**, 182-190.
9. G. Pagano, M. Guida, F. Tommasi and R. Oral, *Ecotoxicol. Environ. Saf.*, 2015, **115**, 40-48.

10. X. Zhang, W. Liu, G. Z. Wei, D. Banerjee, Z. Hu and J. Li, *J. Am. Chem. Soc.*, 2014, **136**, 14230-14236.
11. W. Liu, Y. Fang and J. Li, *Adv. Funct. Mater.*, 2018, **28**, 1705593.
12. V. W.-W. Yam, V. K.-M. Au and S. Y.-L. Leung, *Chem. Rev.*, 2015, **115**, 7589-7728.
13. W. Liu, W. P. Lustig and J. Li, *EnergyChem*, 2019, **1**, 100008.
14. H. Araki, K. Tsuge, Y. Sasaki, S. Ishizaka and N. Kitamura, *Inorg. Chem.*, 2005, **44**, 9667-9675.
15. C. Chen, R.-H. Li, B.-S. Zhu, K.-H. Wang, J.-S. Yao, Y.-C. Yin, M.-M. Yao, H.-B. Yao and S.-H. Yu, *Angew. Chem. Int. Ed.*, 2018, **57**, 7106-7110.
16. X. Hei, W. Liu, K. Zhu, S. J. Teat, S. Jensen, M. Li, D. M. O'Carroll, K. Wei, K. Tan, M. Cotlet, T. Thonhauser and J. Li, *J. Am. Chem. Soc.*, 2020, **142**, 4242-4253.
17. W. Liu, K. Zhu, S. J. Teat, G. Dey, Z. Shen, L. Wang, D. M. O'Carroll and J. Li, *J. Am. Chem. Soc.*, 2017, **139**, 9281-9290.
18. Y. Fang, C. A. Sojdak, G. Dey, S. J. Teat, M. Li, M. Cotlet, K. Zhu, W. Liu, L. Wang, D. M. ÓCarroll and J. Li, *Chem. Sci.*, 2019, **10**, 5363-5372.
19. Y. Fang, W. Liu, S. J. Teat, G. Dey, Z. Shen, L. An, D. Yu, L. Wang, D. M. O'Carroll and J. Li, *Adv. Funct. Mater.*, 2017, **27**, 1603444.
20. W. Liu, K. Zhu, S. J. Teat, B. J. Deibert, W. Yuan and J. Li, *J. Mater. Chem. C*, 2017, **5**, 5962-5969.
21. W. Liu, Y. Fang, G. Z. Wei, S. J. Teat, K. Xiong, Z. Hu, W. P. Lustig and J. Li, *J. Am. Chem. Soc.*, 2015, **137**, 9400-9408.
22. T.-L. Yu, Y.-M. Guo, G.-X. Wu, X.-F. Yang, M. Xue, Y.-L. Fu and M.-S. Wang, *Coord. Chem. Rev.*, 2019, **397**, 91-111.
23. M. Knorr, A. Pam, A. Khatyr, C. Strohmann, M. M. Kubicki, Y. Rousselin, S. M. Aly, D. Fortin and P. D. Harvey, *Inorg. Chem.*, 2010, **49**, 5834-5844.
24. J.-J. Shen, X.-X. Li, T.-L. Yu, F. Wang, P.-F. Hao and Y.-L. Fu, *Inorg. Chem.*, 2016, **55**, 8271-8273.
25. S.-L. Li, F.-Q. Zhang and X.-M. Zhang, *Chem. Commun.*, 2015, **51**, 8062-8065.
26. S. Chen, J. Gao, J. Chang, Y. Li, C. Huangfu, H. Meng, Y. Wang, G. Xia and L. Feng, *ACS Appl. Mater. Interfaces*, 2019, **11**, 17513-17520.
27. J.-J. Hou, S.-L. Li, C.-R. Li and X.-M. Zhang, *Dalton Trans.*, 2010, **39**, 2701-2707.
28. S.-L. Li and X.-M. Zhang, *Inorg. Chem.*, 2014, **53**, 8376-8383.
29. A. N. Hong, H. Yang, A. Zhou, X. Bu and P. Feng, *Cryst. Growth Des.*, 2020, **20**, 6668-6676.
30. A. V. Artem'ev, E. A. Pritchina, M. I. Rakhmanova, N. P. Gritsan, I. Y. Bagryanskaya, S. F. Malysheva and N. A. Belogorlova, *Dalton Trans.*, 2019, **48**, 2328-2337.
31. J.-J. Wang, C. Chen, W.-G. Chen, J.-S. Yao, J.-N. Yang, K.-H. Wang, Y.-C. Yin, M.-M. Yao, L.-Z. Feng, C. Ma, F.-J. Fan and H.-B. Yao, *Journal of the American Chemical Society*, 2020, **142**, 3686-3690.
32. L. Protesescu, S. Yakunin, M. I. Bodnarchuk, F. Krieg, R. Caputo, C. H. Hendon, R. X. Yang, A. Walsh and M. V. Kovalenko, *Nano Lett.*, 2015, **15**, 3692-3696.
33. S.-T. Ha, R. Su, J. Xing, Q. Zhang and Q. Xiong, *Chem. Sci.*, 2017, **8**, 2522-2536.
34. Q. A. Akkerman, V. D'Innocenzo, S. Accornero, A. Scarpellini, A. Petrozza, M. Prato and L. Manna, *J. Am. Chem. Soc.*, 2015, **137**, 10276-10281.
35. D. P. McMeekin, G. Sadoughi, W. Rehman, G. E. Eperon, M. Saliba, M. T. Hörantner, A. Haghighirad, N. Sakai, L. Korte, B. Rech, M. B. Johnston, L. M. Herz and H. J. Snaith, *Science*, 2016, **351**, 151.
36. R. Roccanova, A. Yangui, H. Nhalil, H. Shi, M.-H. Du and B. Saparov, *ACS Appl. Electron. Mater.*, 2019, **1**, 269-274.
37. Z. Luo, Q. Li, L. Zhang, X. Wu, L. Tan, C. Zou, Y. Liu and Z. Quan, *Small*, 2020, **16**, 1905226.
38. L. Lian, M. Zheng, P. Zhang, Z. Zheng, K. Du, W. Lei, J. Gao, G. Niu, D. Zhang, T. Zhai, S. Jin, J. Tang, X. Zhang and J. Zhang, *Chem. Mater.*, 2020, **32**, 3462-3468.
39. I. D. L. Albert, T. J. Marks and M. A. Ratner, *J. Am. Chem. Soc.*, 1997, **119**, 6575-6582.
40. H. Ohara, A. Kobayashi and M. Kato, *Dalton Trans.*, 2014, **43**, 17317-17323.
41. M. Xie, C. Han, Q. Liang, J. Zhang, G. Xie and H. Xu, *Sci. Adv.*, 2019, **5**, eaav9857.
42. A. Tsuboyama, K. Kuge, M. Furugori, S. Okada, M. Hoshino and K. Ueno, *Inorg. Chem.*, 2007, **46**, 1992-2001.
43. C. K. Ryu, M. Vitale and P. C. Ford, *Inorg. Chem.*, 1993, **32**, 869-874.
44. T. Hofbeck, U. Monkowius and H. Yersin, *J. Am. Chem. Soc.*, 2015, **137**, 399-404.
45. J. C. Stewart, D. S. Matthew, J. P. Chris, J. H. Phil, I. J. P. Matt, R. Keith and C. P. Mike, *Z. Kristallogr. Cryst. Mater.*, 2005, **220**, 567-570.
46. J.-H. Jia, X.-L. Chen, J.-Z. Liao, D. Liang, M.-X. Yang, R. Yu and C.-Z. Lu, *Dalton Trans.*, 2019, **48**, 1418-1426.
47. A. Y. Baranov, A. S. Berezin, D. G. Samsonenko, A. S. Mazur, P. M. Tolstoy, V. F. Plyusnin, I. E. Kolesnikov and A. V. Artem'ev, *Dalton Trans.*, 2020, **49**, 3155-3163.
48. D. M. Zink, M. Bächle, T. Baumann, M. Nieger, M. Kühn, C. Wang, W. Klopper, U. Monkowius, T. Hofbeck, H. Yersin and S. Bräse, *Inorg. Chem.*, 2013, **52**, 2292-2305.
49. M. Iwamura, H. Watanabe, K. Ishii, S. Takeuchi and T. Tahara, *J. Am. Chem. Soc.*, 2011, **133**, 7728-7736.
50. B.-K. Guo, F. Yang, Y.-Q. Wang, Q. Wei, L. Liu, X.-X. Zhong, L. Wang, J.-K. Gong, F.-B. Li, W.-Y. Wong, K. A. Alamry and Y. Zhao, *J. Lumin.*, 2020, **220**, 116963.
51. Q. Wei, H.-T. Chen, L. Liu, X.-X. Zhong, L. Wang, F.-B. Li, H.-J. Cong, W.-Y. Wong, K. A. Alamry and H.-M. Qin, *New J. Chem.*, 2019, **43**, 13408-13417.
52. M. Hashimoto, S. Igawa, M. Yashima, I. Kawata, M. Hoshino and M. Osawa, *J. Am. Chem. Soc.*, 2011, **133**, 10348-10351.
53. W. F. McDonough and S. s. Sun, *Chem. Geol.*, 1995, **120**, 223-253.

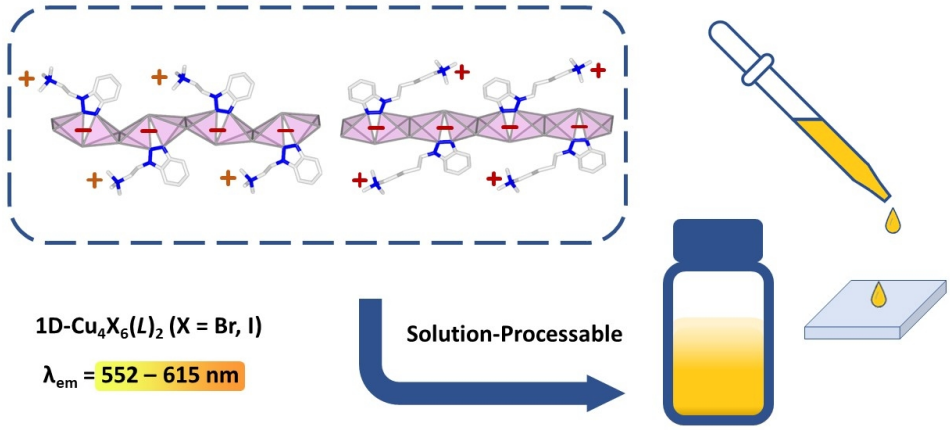

338x190mm (96 x 96 DPI)